Int. J. Multiphase Flow, Vol. 3, pp. 123–139. Pergamon/Elsevier, 1976. Printed in Great Britain.

FLOW OF A PARTICULATE SUSPENSION IN THE WAKE OF A CIRCULAR CYLINDER

D. L. FENTON† and J. J. STUKEL‡
University of Illinois at Urbana-Champaign, Urbana, IL 61801, U.S.A.

(*Received* 8 *August* 1975)

Abstract—Measurements are reported for the average local particulate velocity and concentration distributions in the wake of a cylinder immersed in a stream containing a polydisperse aerosol. The wake centerline defects and transverse distributions were determined for both parameters. It was found that the particulate centerline defect persists a considerable distance downstream of the cylinder before fully developed conditions are satisfied. Transverse particulates and gaseous velocity distributions assume a Gaussian profile at the same point downstream. The charge-to-mass ratio throughout the wake region was equal to the free stream value for all experimental conditions and was of such a magnitude to permit the electrostatic effects to be neglected in the governing equations. Gaseous and particulate transport properties were identified in the wake.

INTRODUCTION

As yet, only one investigation has been reported in the literature involving multiphase flow in a wake region (Deich *et al.* 1973). This work was experimental in nature where the condensation of water vapor in the swirling wake region following a long flat plate was studied. The mean velocity of the gaseous phase was of such magnitude as to be in the compressible flow regime and the phase changes of the water vapor were of interest. Consequently, relevance to the work presented here is not great.

It is well known in gaseous wake flow studies that at sufficient distances downstream, peculiarities in the object geometry become unimportant. In addition, no new wake characteristics can be generated by special object geometries. For these reasons, most researchers have chosen the circular cylinder. This study also employs the circular cylinder not only for the same of simplicity but so that gaseous results in the wake region can be compared directly to the literature. Also to be noted is that this type of unrestricted turbulent wake flow can also be found in jets and within boundary layers on the free side.

GOVERNING EQUATIONS

The coordinate system utilized in formulating the conservation equations for the two-dimensional plane wake is defined as follows: the x-coordinate is positive downstream along the wake axis and is zero at the center of the circular cylinder. The y-coordinate is also zero at the center of the circular cylinder and is positive in the vertical direction.

The motion of the gaseous phase is assumed incompressible which is justified upon consideration of the experimental conditions. The steady-state continuity relations for the fluid and particulate phases become

$$\frac{\partial u}{\partial x}+\frac{\partial v}{\partial y}=0, \qquad [1]$$

$$\frac{\partial}{\partial x}(\rho_p u_p)+\frac{\partial}{\partial y}(\rho_p v_p)=0 \qquad [2]$$

†IIT Research Institute, 10 West 35th Street, Chicago, IL 60616, U.S.A.
‡Professor of Mechanical Engineering and Civil Engineering.

under the restriction of no phase transformations and no internal generation. In the above expressions, u, u_p, v, and v_p are the x and y components of the mean gaseous and particulate phase velocities, respectively, x and y are the free stream and transverse-flow coordinates, and ρ_p is the particulate density. The momentum equations for the fluid and particulate phases in the x-direction are after simplification

$$\rho u \frac{\partial u}{\partial x} + \rho v \frac{\partial u}{\partial y} = + \frac{\partial \tau}{\partial y}, \qquad [3]$$

$$\rho_p u_p \frac{\partial u_p}{\partial x} + \rho_p v_p \frac{\partial u_p}{\partial y} = F\rho_p (u - u_p) + \frac{\rho}{\epsilon_0} p E_x \left(\frac{q}{m}\right)_p + \frac{\partial \tau_p}{\partial y} \qquad [4]$$

where F is the time constant for momentum transfer between the particle and gas, τ and τ_p are the shearing stress of the gaseous and particulate phases, E_x is the x-component of the electric field, $(q/m)_p$ is the charge to mass ratio, ρ is the gaseous density and ϵ_0 is the permittivity of free space.

For turbulent flow, the velocities u and v are to be interpreted as mean velocities. Since the constitutive equation for τ has not been specified, the gaseous momentum equation is not restricted to laminar flow. For the reason that the main flow velocity is large relative to the transverse velocity in wake flow, the y component of fluid momentum is neglected (Hinze 1959). The mean pressure variation is small in the y-direction. In the x-direction, the mean pressure conforms to the pressure distribution in the main flow. The pressure distribution in the main flow in this investigation is uniform; therefore, the mean pressure is constant throughout the entire wake region.

With the assumption of a dilute suspension, [2] in combination with Fick's Law is

$$u \frac{\partial \rho_p}{\partial x} + v \frac{\partial \rho_p}{\partial y} = -\frac{\partial}{\partial y}\left[\left(\frac{q}{m}\right)_p \frac{E_y \rho_p}{F\epsilon_0}\right] + \frac{\partial}{\partial y}\left[\epsilon_{cp} \frac{\partial \rho_p}{\partial y}\right] \qquad [5]$$

where mass diffusion in the x-direction is taken to be much less than in the y-direction, E_y is the y-component of the electric field and ϵ_{cp} is the eddy-diffusion coefficient for the particulate density. Also, [5] includes diffusion by an electric field force.

The interparticle spacing in this investigation is sufficient to prohibit the particulate phase to influence the motion of the gaseous phase. For this case, the gaseous motion is uncoupled from the particulate phase motion.

Boundary conditions for the gaseous phase are as follows:

$$y = 0, \quad \frac{\partial u}{\partial y} = 0, \quad v = 0,$$

$$y \to \pm\infty, \quad u = u_\infty, \quad v = 0.$$

Defining u_1 as the mean velocity deviation behind the circular cylinder and upstream velocity, the equation of motion in the x-direction becomes

$$\frac{\partial}{\partial x}\frac{u_1}{u_\infty} = \frac{\partial}{\partial y}\frac{\tau}{\rho u_\infty^2}. \qquad [6]$$

By assuming

$$\tau_{xy} = \rho \epsilon_{mR} \frac{\partial u_1}{\partial y}$$

where ϵ_{mg} is the coefficient of eddy viscosity for the gaseous phase and following the work of Hinze (1959), [6] can be rewritten as

$$\frac{u_1}{u_{1\max}} = \exp\left[-\frac{u_\infty d}{2}\int_0^n \frac{1}{\epsilon_{mg}}\,\eta\,\mathrm{d}\eta\right] \qquad [7]$$

where d is the diameter of the circular cylinder. The integral in [7] can be evaluated if ϵ_{mg} is prescribed. The simplest case occurs when ϵ_{mg} is constant. Carrying out the integration for this case yields

$$\frac{u_1}{u_{1\max}} = \exp\left[-\frac{u_\infty d}{4\epsilon_{mg}}\,\eta^2\right], \qquad [8]$$

where

$$\eta \equiv \frac{y}{\sqrt{d(x+x_0)}}.$$

Another result is that

$$\frac{u_{1\max}}{u_\infty} = \frac{C}{\sqrt{\xi}}$$

where

$$\xi \equiv \frac{x+x_0}{d},$$

C is a constant and x_0 is the geometrical origin of similarity of the wake.

The momentum equation in the x-direction for the particulate phase, again interpreting velocities as mean quantities, is

$$u_p\frac{\partial u_p}{\partial x} + \frac{\partial u_p}{\partial y} = F(u-u_p) + \frac{E_x}{\epsilon_0}\left(\frac{q}{m}\right)_p + \epsilon_{mp}\frac{\partial^2 u_p}{\partial y^2} \qquad [9]$$

where for turbulent flow

$$\tau_p = \rho_p \epsilon_{mp}\frac{\partial u_p}{\partial y}$$

which is taken to be analogous to the gaseous phase. ϵ_{mp} is the eddy-diffusion coefficient for the particulate phase momentum.

Proceeding in a manner which is analogous to the gaseous phase, assuming that the relaxation time for the particles is small and that electrostatic forces can be neglected, gives

$$\frac{u_{p1}}{u_{p1\max}} = \exp\left[-\frac{u_{p\infty} d}{4\epsilon_{mp}}\,\eta^2\right] \qquad [10]$$

where the integration is performed under the condition that ϵ_{mp} is a constant scaler. It should be noted that the above can be written as

$$\frac{\epsilon_{mp}}{u_{p\infty}d} = \frac{-\frac{1}{2}\eta\frac{u_{p1}}{u_{p1\max}}}{\frac{d}{d\eta}\left(\frac{u_{p1}}{u_{p1\max}}\right)}.$$

In addition

$$\frac{u_{p1\max}}{u_{p\infty}} = \frac{C_p}{\sqrt{\xi}}$$

where C_p is a constant.

A tacit assumption has been made concerning the particulate phase—that the geometrical origins of similarity for both the gaseous and particulate phases coincide. This is reasonable upon realization that the gaseous phase "drags" the particulate phase to the extent (in the absence of boundaries) that the particulate velocity distribution would be expected to approximate the gaseous velocity distribution in shape.

Next, take ρ_{p1} as the mean deviation of local particulate density from the free stream particulate density. Also, let the perturbation in the particulate density ρ_{p1} and the velocity v be indicated by $\boldsymbol{\rho}_{p1}$ and $\mathbf{v}$ respectively. Making the assumption that the contribution of molecular transport is much less than the turbulent contribution and following the approach of Townsend (1956) gives

$$u_\infty\frac{\partial\rho_{p1}}{\partial x} = -\frac{\partial}{\partial_y}\overline{\mathbf{v}\boldsymbol{\rho}_{p1}}$$

where the bar indicates the time mean average. Under the assumption that the transport of ρ_p is analogous to the transport of gaseous momentum

$$-\overline{\mathbf{v}\boldsymbol{\rho}_{p1}} = \epsilon_{cp}\frac{\partial\rho_{p1}}{\partial y}$$

where ϵ_{cp} is an unprescribed scaler. Since the transport of ρ_p is assumed analogous, similar profiles in the wake region should exist. Borrowing the solution for the gaseous momentum distribution in the wake region, ϵ_{cp} can be written as

$$\frac{\epsilon_{cp}}{u_\infty d} = \frac{-\frac{1}{2}\eta\frac{\rho_{p1}}{\rho_{p1\max}}}{\frac{d}{d\eta}\left(\frac{\rho_{p1}}{\rho_{p1\max}}\right)}.$$

As done before, integration yields

$$\frac{\rho_{p1}}{\rho_{p1\max}} = \exp-\frac{u_\infty d}{2}\int_0^\eta\frac{\eta\,d\eta}{\epsilon_{cp}} \qquad [11]$$

whereupon if ϵ_{cp} is considered to be a constant

$$\frac{\rho_{p1}}{\rho_{p1\max}} = \exp-\frac{u_\infty d}{4\epsilon_{cp}}\eta^2 \qquad [12]$$

which again is Gauss's function. From solutions [10] and [12]

$$\frac{\rho_{p1}}{\rho_{p1\max}} = \left(\frac{u_{p1}}{u_{p1\max}}\right)^{\epsilon_{mp}/\epsilon_{cp}}. \qquad [13]$$

To be noted is that [13] can also be obtained from [10] before the integration is carried through [11] and if $\epsilon_{mp}/\epsilon_{cp}$ is constant throughout the particulate wake flow region.

Consider next the following integral transformations (Schlichting 1968):

$$\delta^* \equiv \int_{-b_g}^{+b_g} \left(1 - \frac{u}{u_\infty}\right) \mathrm{d}y,$$

$$\theta \equiv \int_{-b_g}^{+b_g} \frac{u}{u_\infty}\left(1 - \frac{u}{u_\infty}\right) \mathrm{d}y$$

where b_g is half of the total gaseous wake width at the point where $u_1 = 0.01\, u_\infty$. Substituting the above variables into [3] and assuming a zero pressure gradient gives:

$$\frac{\mathrm{d}}{\mathrm{d}x}(\theta + \delta^* - 2b_g) = 0.$$

Similarly, integral transformations for the particulate phase can be defined as follows:

$$\delta_p^{*\prime} \equiv \int_{-b_p}^{+b_p} \left(1 - \frac{\rho_p u_p}{\rho_{p\infty} u_{p\infty}}\right) \mathrm{d}y,$$

$$\theta_p \equiv \int_{-b_p}^{+b_p} \frac{\rho_p u_p}{\rho_{p\infty} u_{p\infty}}\left(1 - \frac{u_p}{u_{p\infty}}\right) \mathrm{d}y,$$

$$\delta'_{pg} \equiv \int_{-b_p}^{+b_p} \left(1 - \frac{\rho_p u}{\rho_{p\infty} u_\infty}\right) \mathrm{d}y,$$

$$\delta_e \equiv \int_{-b_p}^{+b_p} \left[1 - \frac{\rho_p E_x (q/m)_p}{\rho_{p\infty} E_{x\infty} (q/m)_{p\infty}}\right] \mathrm{d}y$$

where b_p is half of the total particulate velocity wake width at the point where $u_{p_1} = 0.01\, u_{p\infty}$.

Substituting these variables into [4] and assuming $u_\infty = u_{p\infty}$, a zero pressure gradient and F constant yields:

$$\frac{\mathrm{d}}{\mathrm{d}x}(\theta_p + \delta^{*\prime}) = 2\frac{\mathrm{d}b_p}{\mathrm{d}x} + \frac{F}{u_\infty}(\delta'_{pg} - \delta_p^{*\prime}) + E_{x\infty}\left(\frac{q}{m}\right)_{p\infty}(\delta_e - 2b_p). \qquad [14]$$

The above expression is valid for both laminar and turbulent flow. Integration of the particulate diffusion utilizing the definition of δ'_{pb} yields

$$\frac{\mathrm{d}}{\mathrm{d}x}(\delta'_{pg}) = 2\frac{\mathrm{d}b_c}{\mathrm{d}x} + \frac{1}{\epsilon_0}\left(\frac{q}{m_p}\right)_p^2 \frac{\rho_{p\infty}}{u_\infty F}(2b_c - \delta_c). \qquad [15]$$

Applying particulate continuity to a control volume which extends upstream some distance from the circular cylinder and downstream parallel to the flow direction over the width of the particulate wake gives the following result after rearrangement:

$$\frac{m_{0_p}}{\rho_{p\infty} u_{p\infty}} = 2\left[1 - \int_0^1 \frac{\rho_p u_p}{\rho_{p\infty} u_{p\infty}} \mathrm{d}\left(\frac{y}{b}\right)_p\right] = 2\delta_p^{*\prime} \qquad [16]$$

where m_{0_p} is the particulate mass flux spillage from the control volume. Going through the

identical procedure with the same control volume for the gaseous phase results in

$$\frac{m_{0g}}{\rho_\infty u_\infty} = 2\left[1 - \int_0^1 \frac{\rho u}{\rho_\infty u_\infty} \mathrm{d}\left(\frac{y}{b}\right)_g\right] = 2\delta^* \qquad [17]$$

where m_{0g} is the gaseous mass flux spillage from the control volume. Combining [16] and [17] results in

$$\left(\frac{\rho_\infty u_\infty}{\rho_{p_\infty} u_{p_\infty}}\right)\left(\frac{m_{0p}}{m_{0g}}\right) = \frac{1 - \int_0^1 \frac{\rho_p u_p}{\rho_{p_\infty} u_{p_\infty}} \mathrm{d}\left(\frac{y}{b}\right)_p}{1 - \int_0^1 \frac{\rho u}{\rho_\infty u_\infty} \mathrm{d}\left(\frac{y}{b}\right)_p} = \frac{\delta^*}{\delta_p^{*\prime}}.$$

For the purpose of the design of experiments and the interpretation of experimental results, it is of interest to nondimensionalize the governing equations. Introducing the following nondimensional variables

$$x^+ = \frac{x}{d} \qquad u_p{}^+ = \frac{u_p}{u_{p_\infty}} \qquad F^+ = \frac{F}{F_\infty} \qquad u^+ = \frac{u}{u_\infty},$$

$$y^+ = \frac{y}{d} \qquad v_p{}^+ = \frac{v_p}{u_{p_\infty}} \qquad \rho^+ = \frac{\rho_p}{\rho_{p_\infty}} \qquad v^+ = \frac{v}{u_\infty},$$

$$E_x{}^+ = \frac{E_x}{E_\infty} \quad \left(\frac{q}{m}\right) = \frac{(q/m)_p}{(q/m)_{p_\infty}} \qquad E_y{}^+ = \frac{E_y}{E_\infty}$$

into [4] yields

$$u_p{}^+ \frac{\partial u_p{}^+}{\partial x^+} + v_p{}^+ \frac{\partial u_p{}^+}{\partial y^+} = \frac{F^+}{N_m}(u^+ - u_p{}^+) + \left(\frac{N_{ev}}{N_R}\right)^2 E_x{}^+ \left(\frac{q}{m}\right)_p^+ + (N_D)_d \frac{\partial^2 u_p{}^+}{\partial y^{+2}}$$

in which ϵ_{mp} is assumed constant and when the dimensionless groups are defined as

$$(N_m)_d \equiv \frac{u_{p_\infty}}{F_\infty d} \quad (N_R)_d \equiv \frac{u_{p_\infty} d}{\nu} \quad (N_{ev})_d \equiv \left(\frac{\rho_{p_\infty}}{2\pi\epsilon_0}\right)^{1/2} \frac{d^2}{\epsilon_{mg}} \left(\frac{q}{m}\right)_{p_\infty}$$

$$(N_D)_{md} \equiv \frac{\epsilon_{mp}}{u_{p_\infty} d}.$$

Consequently, the appropriate dimensionless groups for the particulate phase are $(N_m)_d$, $(N_R)_d$, $(N_{ev})_d$, and $(N_D)_{md}$ and are not merely $(N_R)_d$ as with the gaseous phase. In the above equations, the term due to electrostatic effects can be neglected if $(N_{ev})_d \ll (N_R)_d$.

The particulate diffusion equation can also be nondimensionalized with the same procedure. The result is

$$u^+ \frac{\partial \rho_p{}^+}{\partial x^+} + v^+ \frac{\partial \rho_p{}^+}{\partial y^+} = -\frac{(N_{ev})_d^2 (N_m)_d}{(N_R)_d^2} \frac{\partial}{\partial y^+} \frac{E_y{}^+}{F^+} \left(\frac{q}{m}\right)_p^+ \rho_p{}^+ + (N_D)_{cd} \frac{\partial^2 \rho_p}{\partial y^{+2}}$$

where ϵ_{cp} is assumed constant and

$$(N_D)_{cd} \equiv \frac{\epsilon_{cd}}{u_\infty d}.$$

In the particulate diffusion equation, the electrostatic field effects due to the presence of charged particles can be neglected if

$$(N_{ev})_d^2(N_m)_d \ll (N_R)_d^2.$$

EXPERIMENTAL PROCEDURE AND APPARATUS

The experimental system used for this investigation was a recirculation type wind tunnel. By proper selection of the fan motor speed and damper control, Reynolds numbers based on the duct's hydraulic diameter ranging from 5.6×10^4 to 6.4×10^5 were obtained. The entire wind tunnel was electrically grounded.

The gaseous velocity was measured with a modified Prandtl pitotstatic tube. Conventional inclined differential manometers were used to indicate the dynamic pressure. The resolution of these manometers was at least 0.0127×10^{-2} m of water. All gaseous velocity measurements performed in the absence of particles in suspension utilized the pitotstatic tube. Gaseous velocities were also required in the suspension flow itself. Plugging of the pitot-static tube rendered this instrument unusable. Morr (1972) developed a counterflow technique which allowed the measurement of the gaseous phase velocity profile in the gas–solid suspension. This probe was used for gaseous wake profiles.

Mass flux measurements were made using standard isokinetic sampling methods. The particulate material was filtered from the gas by Whatman cellulose extraction thimbles. The filtering efficiency for this thimble was 100% for particles greater than 2 μm in diameter.

The particulate concentration was measured using a fiber optic probe. This probe is described by Fenton & Stukel (1976).

The introduction cited experiments in the literature which indicated that in a dilute suspension, the gaseous flow field was not influenced. These experiments, though, were only concerned with fully developed pipe flow and jet flow. Consequently, experiments were performed downstream from the circular cylinder in the gaseous wake flow region utilizing a counterflow probe developed by Morr (1972) to establish the influence of the particulate phase on the gaseous phase. In figure 1, results are shown for the axial gaseous wake velocity for various distances downstream at different free stream particulate loadings. From these results, moderate particulate loadings are not seen to alter the axial velocity in the wake. Figure 2 shows the effects of particulate loading upon distribution of gaseous velocity within the wake region under conditions where similarity is established. Indications are that particulate loading conditions in the experiments reported in this work do not alter substantially the mean characteristics of the gaseous wake flow in the region of similarity.

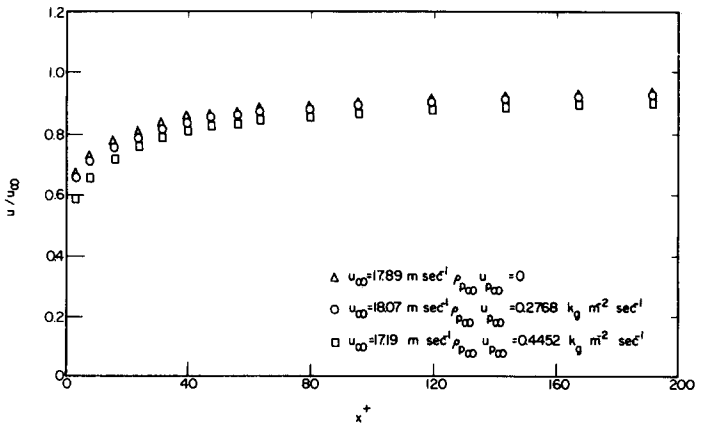

Figure 1. Gaseous velocity along wake axis with particulate loading for $d = 3.175 \times 10^{-3}$ m.

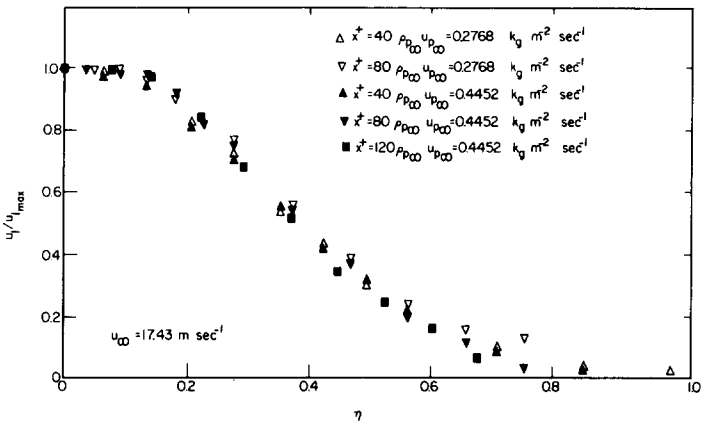

Figure 2. Gaseous wake profile as influenced by particulate loading for $d = 3.175 \times 10^{-3}$ m.

In the theoretical development for the gaseous flow, a similar solution was sought and obtained. Resulting from this analysis were functions which characterized the mean flow in the wake region,

$$\frac{u_{1\max}}{u_\infty} = C\frac{1}{\sqrt{\xi}},$$

$$\frac{u_1}{u_{1\max}} = \exp\left[-\frac{u_\infty d}{4\epsilon_{mg}}\eta^2\right]$$

where

$$\xi = \frac{x + x_0}{d} \quad \text{and} \quad \eta = \frac{y}{\sqrt{d(x + x_0)}}.$$

The variable η is the similarity variable where x_0 is the location of the geometrical origin of similarity. By momentum and energy considerations, Townsend (1956) determined the location of the "effective" origin, realizing that self-preservation can only be approximate. Employing Townsend's results, the effective origin was calculated to be $x_0/d = 9.0$. This value is used throughout the discussion of the gaseous phase results.

The above equations predict that the gaseous velocity defect along the wake axis normalized with the free stream velocity is proportional to $\xi^{-1/2}$. This prediction is supported by the data in figure 3. Although the constant of proportionality is different for each measurement condition, proportionality is well established for values of $x/d > 40$. Equation[9] predicts that the distribution of gaseous velocity within the wake region should be Gaussian. Typical results are shown in figure 4. These results coincide with those made for $2.40 \times 10^3 < N_{R_D} < 6.93 \times 10^3$. Measurements made of the gaseous velocity profile for $x/d < 40$ deviate from the profiles measured further downstream. Thus, similarity is seen to exist for distances greater than $x/d = 40$ for the gaseous wake. The curves drawn on the gaseous wake profiles are results of [8] choosing the appropriate ξ_{mg} which best satisfies the experimental points. For the most part, the central portion of the wake behaves as predicted by this gradient-type diffusion concept of transport. It should be noted that even though this concept does give an adequate prediction of meanmomentum distribution, it does not provide insight to the real physical processes which are occurring in the wake itself. At the outer wake boundaries, agreement with the Gaussian distribution is not good. In this region of the wake, the apparent coefficient of eddy diffusion is much smaller than the assumed fixed value obtained from the central portion of the wake. This, however, for the purposes of this work is not considered serious. Table 1 presents a summation

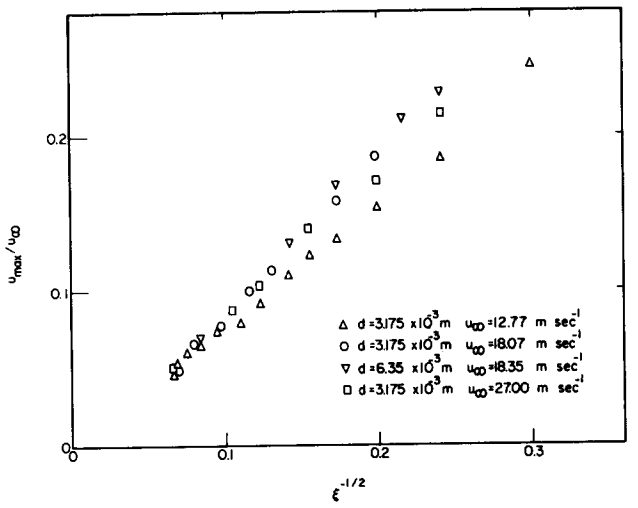

Figure 3. Gaseous velocity along wake axis.

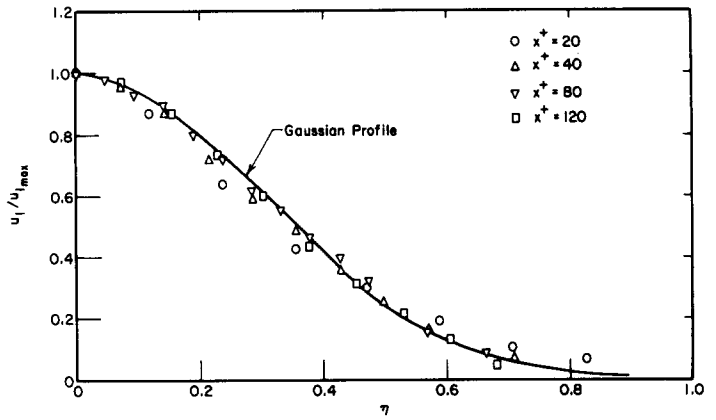

Figure 4. Gaseous wake profile at $u_\infty = 27.0$ m s^{-1} for $d = 3.175 \times 10^{-3}$ m.

Table 1. Eddy-transport coefficients

u_∞ (m s^{-1})	d (m)	ρ^*_∞	$\frac{2\epsilon_m}{u_\infty L}$	$\frac{\epsilon_{mg}}{u_\infty d}$	$\frac{\epsilon_{mp}}{\epsilon_{mg}}$	$\frac{\epsilon_{cp}}{\epsilon_{mg}}$	$\frac{\epsilon_{mp}}{\epsilon_{cp}}$
12.68	3.175×10^{-3}	0.0141	1.41×10^{-4}	0.0481	0.489	0.632	0.773
18.07	3.175×10^{-3}	0.00657	1.41×10^{-4}	0.0481	0.469	0.675	0.695
18.07	3.175×10^{-3}	0.0155	1.41×10^{-4}	0.0481	0.589	0.698	0.700
18.26	6.35×10^{-3}	0.00657	1.41×10^{-4}	0.0418	0.608	0.804	0.755
18.26	6.35×10^{-3}	0.0157	1.41×10^{-4}	0.0418	0.653	0.830	0.786
27.0	3.175×10^{-3}	0.0106	1.41×10^{-4}	0.0443	0.551	0.686	0.803
27.0	3.175×10^{-3}	0.0146	1.41×10^{-4}	0.0443	—	0.747	—
27.0	3.175×10^{-3}	0.0232	1.41×10^{-4}	0.0443	0.616	0.783	0.787

of the apparent coefficients of eddy diffusion for the gaseous flow. In table 1, ρ^* is the ratio of the local particulate density to the gaseous density.

Also to be noted is that since the gaseous wake profiles coalesce for all Reynolds numbers tested in the region of similarity, no peculiarities occur in the flow about the circular cylinder. Looking back to figure 3 rather dramatically demonstrates nonuniformity in close proximity to the circular cylinder. An additional experiment was conducted to ascertain any peculiarities in the duct flow that would influence the gaseous wake. The cylinder was relocated in the vertical plane and the wake generated was measured at $x/d = 80$. Since these data points coincide with the previous data, no apparent influence of the duct flow is observed.

Figures 5 and 6 present the growth of the gaseous wake half width, b_{2g}. C_d is the drag coefficient of the cylinder. The same data are used for both plots, but figure 6 corresponds in format to other published results (Schlichting 1968). Since the data generalize to a straight line, the half width varies exponentially with downstream distances which is in accord with other results. Figure 5 is included for comparisons that will be made with the particulate wake characteristics.

Measurement of the particulate charge-to-mass ratio $(q/m)_p$ was performed at all experimental conditions. In table 2, the free stream charge-to-mass ratio $(q/m)_{p_\infty}$ corresponded to the experimental conditions indicated. The charge-to-mass ratio, though not a function of the particulate density, does depend on gaseous velocity. Throughout the particulate wake region, the charge-to-mass ratio maintained the free stream value.

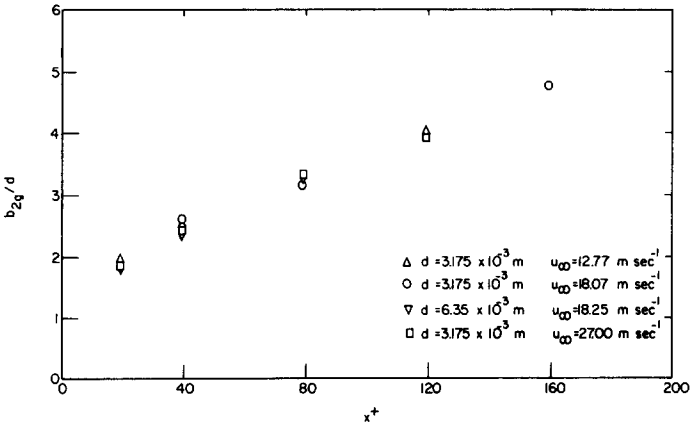

Figure 5. Gaseous wake half width.

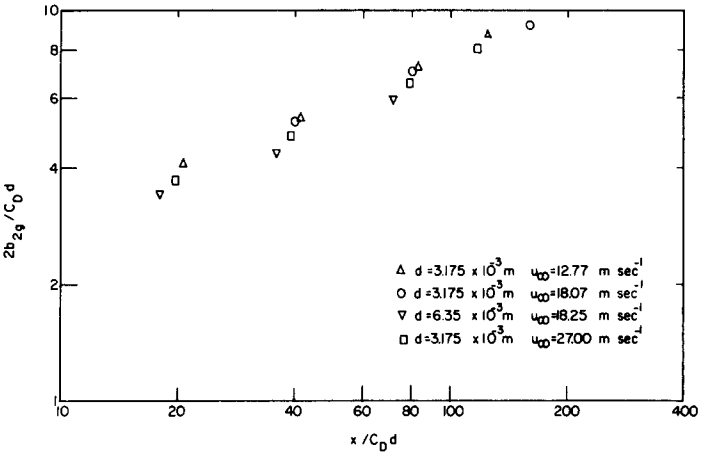

Figure 6. Gaseous wake half width based on drag coefficient.

Table 2. Duct centerline characteristics for experimental conditions

u (m s^{-1})	d (m)	ρ_∞^*	$\rho_{p_\infty} u_{p_\infty}$ (kg m^{-2} s^{-1})	$\left(\frac{q}{m}\right)_{p_\infty}$ (coul kg^{-1})
12.68	3.175×10^{-3}	0.0141	0.1777	2.64×10^{-4}
18.07	3.175×10^{-3}	0.00657	0.1279	10.00×10^{-4}
18.07	3.175×10^{-3}	0.0155	0.4228	10.67×10^{-4}
18.26	6.35×10^{-3}	0.00657	0.2270	14.46×10^{-4}
18.26	6.35×10^{-3}	0.0157	0.3862	13.12×10^{-4}
27.0	3.175×10^{-3}	0.0106	0.2915	5.97×10^{-3}
27.0	3.175×10^{-3}	0.0232	0.7714	4.67×10^{-3}

As noted earlier, the electrostatic term could be neglected in the governing equations if $(N_{ev})_d \ll (N_R)_d$. Typical values for these dimensionless groups were

$$(N_{ev})_d \sim 10^{-5} \quad \text{and} \quad (N_R)_d \sim 10^3$$

which does justify neglecting the electrostatic term in the particulate equation of motion in this study. Also, recall that electrostatic effects could be neglected in the dimensionless particulate diffusion equation if $(N_{ev})^2(N_m)_d \ll (N_R)_d^2$. This too is justified since typical results indicate

$$(N_{ev})_d^2(N_m)_d \sim 10^{-11} \quad \text{and} \quad (N_R)_d \sim 10^6.$$

In the following discussion, measurements of particulate velocity are presented. With the measurement techniques utilized, particulate velocity was not measured directly but through combination of the particulate mass flux and particulate density measurements. Essentially the local mass flux divided by the particulate density at the same locality yields the particulate velocity. This approach provides no information concerning the relative velocities of different particle sizes.

Recalling the similarity analysis for the particulate phase, solutions for the variance of particulate characteristics along the wake axis and throughout the wake region were determined. Results indicated that

$$\frac{u_{p\,1\max}}{u_{p_\infty}} = C_p \frac{1}{\sqrt{\xi}},$$

$$\frac{u_{p\,1}}{u_{p\,1\max}} = \exp\left[-\frac{u_{p_\infty} d}{4\epsilon_{mp}} \eta^2\right]$$

where ϵ_{mp} was a constant scaler. As discussed earlier, the distribution of particulate density within the wake region should be Gaussian, although not necessarily in the same way as the particulate velocity. Consequently, mathematical forms analogous to the equations above are assumed for the particulate density as well.

Before proceeding beyond this point, discussion concerning the geometrical origin of similarity of the particulate wake—both particulate momentum and density—is in order. The theoretical analysis was based upon the assumption that these virtual origins for the gaseous and particulate wakes coincide. Attempted now will be experimental justification for this assumption. Extrapolating the wake half widths for gaseous flow should indicate the approximate location of the virtual origin and carrying this procedure out, agreement was reasonable (about one cylinder diameter) relative to the calculated virtual origin. Applying this same procedure to the particulate wake, the virtual origins were determined to be in the same vicinity as for gaseous flow allowing for experimental errors. Therefore, throughout this entire discussion, the virtual origin for all wakes was taken to be $x_0/d = 9.0$.

Referring now directly to experimental results, figure 7 shows how the particulate velocity varies along the wake axis for a typical free stream condition. Quite noticeable is the considerable distance downstream before the velocity variation is proportional to $\xi^{-1/2}$. The data suggest that greater distances are required for manifestation of fully developed conditions for particulate velocity. This distance is seen to be approximately $x/d = 80$. Hence, the development of particulate velocity characteristics requires twice the length as development of gaseous flow along the axis.

The variance of particulate density along the wake axis for a typical set of conditions is indicated in figure 8. Again, although not to the extent as with the axial particulate velocity, a greater distance is required before particulate density varies as $\xi^{-1/2}$. The approximate distance

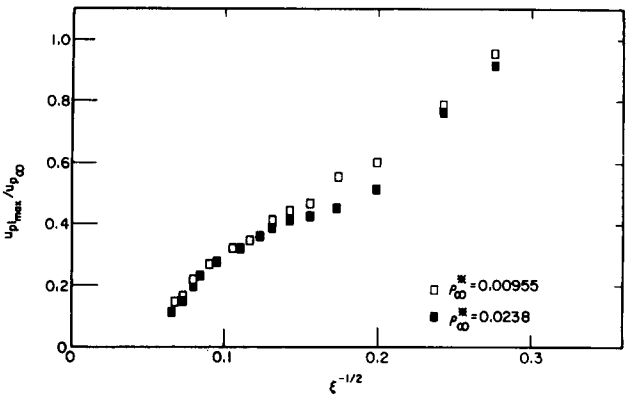

Figure 7. Particulate velocity along wake axis at $u_{p_\infty} = 27.0$ m s^{-1} for $d = 3.175 \times 10^{-3}$ m.

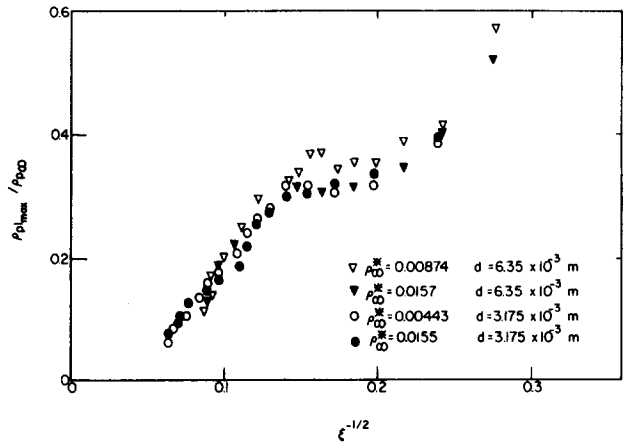

Figure 8. Particulate density along wake axis at $u_{p_\infty} = 18.26$ m s^{-1} for $d = 3.175 \times 10^{-3}$ m.

as deduced from the data is $x/d = 50$–55. Consequently, development of the particulate density characteristics along the wake axis occurs between the gaseous and particulate development.

With the mathematical analysis, particulate momentum was predicted to be distributed in a Gaussian manner. Figure 9 shows a typical result for the actual particulate velocity defect plotted against the gaseous similarity parameter. It was found for all the test conditions that η was an effective similarity parameter for the particulate velocity as well. This is expected, however, in

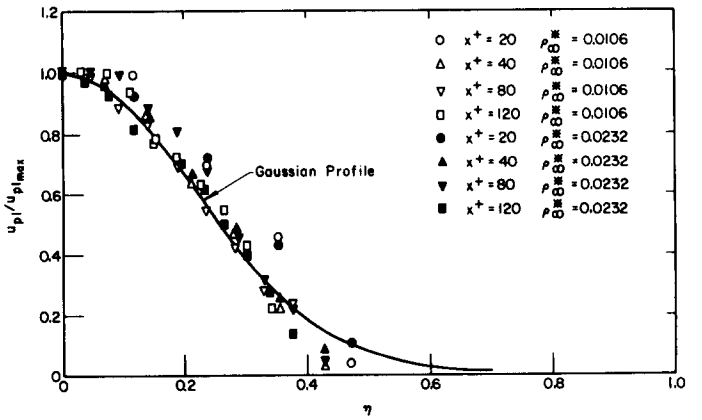

Figure 9. Particulate velocity wake profile at $u_{p_\infty} = 27.0$ m s^{-1} and $d = 3.175 \times 10^{-3}$ m.

that the gas imparts momentum to the particles through drag effects and consequently whatever the gaseous momentum distribution is, the particulate momentum distribution should be at least somewhat similar in shape. The particulate wake velocity profiles plotted are seen to be nearly Gaussian since the line drawn through the data is the Gaussian curve itself choosing the apparent coefficient of eddy diffusion for particulate momentum, ϵ_{mp}. Table 1 gives values of this apparent eddy-diffusion coefficient relative to the coefficient of eddy diffusion for gaseous wake flow. The particulate momentum eddy-diffusion coefficient is roughly half the eddy-diffusion coefficient for gaseous flow for the particulate material employed in this study.

The distribution of particulate momentum within the wake is not influenced by the free stream particulate density. This is seen to be the case for all particulate velocity data. Interesting with the distribution of particulate momentum is the achievement of similarity which is complete at $x/d = 40$, since deviations in the particulate velocity profiles are imperceptible. This is in contrast to conditions along the wake axis which required twice this distance. Remember, though, that in the profile plots, the defect in particulate velocity is normalized with the maximum defect which occurs at the wake axis. Therefore, no information is conveyed concerning the magnitude of the defect, but only how this defect is distributed in the flow field. The gaseous–particulate interaction term in the momentum equation is a maximum at the wake axis and immediately decreases upon movement from the axis. However, note that the coefficient of eddy diffusion for particulate velocity is constant within the central portion of the wake region. Therefore, the turbulent diffusion term in the momentum equation maintains its axial magnitude throughout the wake, thus diminishing the relative influence of the interaction term. This argument further explains the reason for measurement of a Gaussian particulate momentum distribution. Disagreement between the Gaussian curve and the data near the boundary of the wake can be attributed, as in the gaseous wake, to the considerably reduced ϵ_{mp} in this region.

Gaussian distributions were also measured for particulate density defects within the wake region. Figure 10 gives typical results. Again, η, as the similarity parameter, collapses all the test data, indicating its validity. Although similarity is attained at $x/d = 40$, large deviations are noted at $x/d = 20$ for most conditions. Beyond $x/d = 40$, no significant deviations occur except near the wake boundary which can be accounted for in the same way as for the gaseous flow. Table 1 indicates values of the apparent coefficient of eddy diffusion for the particulate density relative to the corresponding gaseous values which in turn were used to generate the actual Gaussian curves superimposed on the experimental data. The ratios of eddy diffusivities for the particulate momentum and density for the various experimental conditions are calculated. Within experimental error, the ratio of $\epsilon_{mp}/\epsilon_{cp}$ is constant (about 0.77) which interestingly enough justifies[13] determined from the integral forms of particulate velocity and momentum defect distributions. Also, the data clearly indicate that the free stream particulate density does not alter the distribution of the particulate density defect.

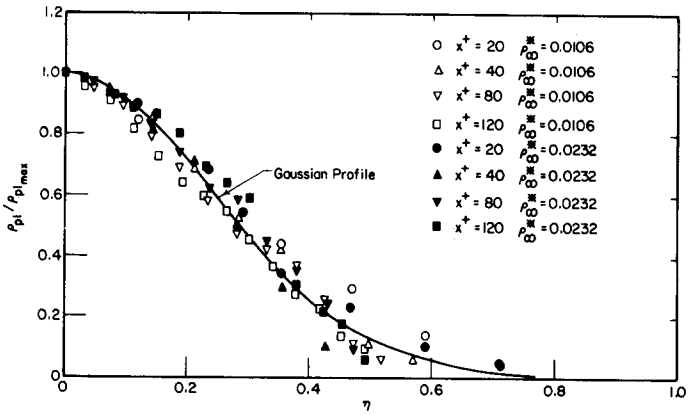

Figure 10. Particulate density wake profile at $u_{p_\infty} = 27.0$ m s^{-1} and $d = 3.175 \times 10^{-3}$ m.

Application of Fick's Law to mass diffusion in the wake region also yields values of ϵ_{cp}. Since effects due to electrostatic forces can be neglected, Fick's Law can be written in the y-direction as

$$J_{py} = -\epsilon_{cp}\frac{\partial \rho_p}{\partial y}$$

where J_{py} is the particulate mass flux displaced by the wake. In the central portion of the wake, $\partial \rho_p / \partial y$ is essentially constant and for the calculations performed, evaluated at the wake half width. The flux, J_{py}, was determined through a particulate mass balance for a control volume about the wake region. Consequently, a check on the apparent coefficient of eddy diffusion for particulate density can be made. Results of this procedure indicate agreement to within 11% of the previously calculated values.

The relationship between the particulate and gaseous wake half widths, b_{2p} and b_{2g}, is indicated in figures 11 and 12. The particulate momentum wake half width and the particulate density half width, b_{2c}, are depicted, respectively. Apparently, growth of both particulate half widths relative to the gaseous half width is large near the cylinder ($20 < x/d < 40$) but further downstream, the growth rate decreases considerably. The measurements made, however, indicate that for $x/d < 120$, both the particulate momentum and particulate density wakes are smaller in width than the gaseous wake. Also observed from this data the approximate agreement of relative half width for the particulate wakes at $x/d = 20$, but as x/d increases from this value, divergence

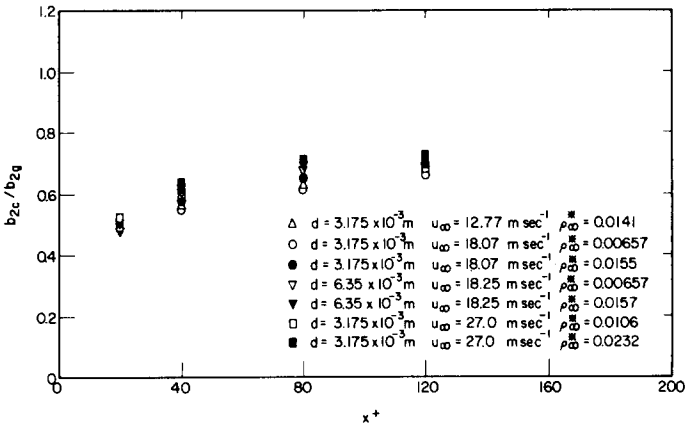

Figure 11. Particulate velocity wake half width relative to gaseous half width.

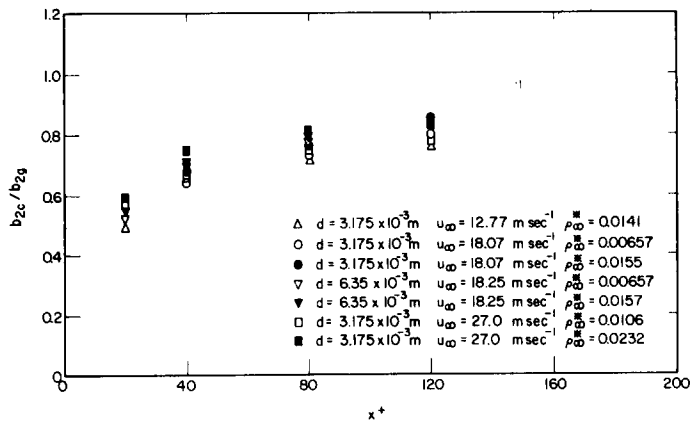

Figure 12. Particulate density wake half width relative to gaseous half width.

increases. This is probably due to the fact that the gaseous flow field is able to distribute particulate density more readily than particulate momentum. Recall that the particulate mass flux measurement would be most sensitive to the large particles and thus influence the particular velocity measurement. However, with measurement of particulate density, the particle size distribution has little effect. Consequently, the indicated growth of the particulate momentum wake half width possesses a preference for the larger particles, thus explaining in part the relative lack of growth. The free stream particulate density is observed to have a slight effect on growth of the particulate density half width. At $x/d = 120$, under the experimental conditions of this work, this amounts to roughly 5% of the gaseous wake half width. Particulate density has no discernible influence on the particulate momentum half width.

Recall that:

$$\frac{d}{dx}(\theta + \delta^* - 2b_g) = 0.$$

Examination of the above equation suggests that since the momentum thickness, θ, is a constant in the wake region of a circular cylinder, the growth of the gaseous displacement thickness, δ^*, should be offset by the growth in the total wake width. Experimental results indicate that θ is constant downstream of the cylinder. This suggests that δ^* and $2b$, must have the same growth rate downstream of the cylinder. Comparing the growth rate of the total wake width with the variation of δ^* reveals that they are indeed the same within experimental error.

The variation of θ_p with downstream distance is shown in figure 13. In contrast to the gaseous-momentum parameter θ, θ_p increases uniformly over the distance measured whereas θ was relatively constant. This suggests that the behavior of the particles in the wake of the cylinder is different from the gaseous phase over the range of the measurements experimental conditions examined in this study.

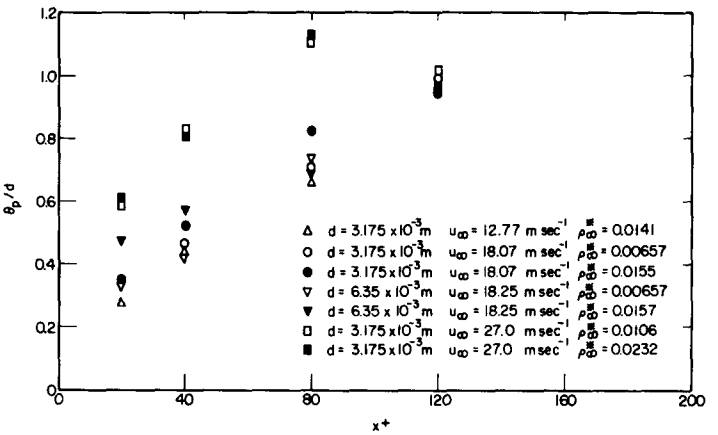

Figure 13. Variation of particulate momentum thickness, θ_p.

The distribution of $\delta_p^{*\prime}$ and δ'_{pg} with downstream distance is shown in figures 14 and 15. It is of interest to note that $\delta_p^{*\prime}$ exhibits a relative maximum at $x^+ \simeq 80$. Recall that by neglecting charge effects the particle diffusion equation can be written as

$$\delta'_{pg} - 2b_c = \text{constant}. \qquad [18]$$

This result is rather remarkable in view of its simplicity and the rather complex nature of particulate suspension flow in a wake region. Only measurement of local gaseous velocity and local particulate density are required to determine δ'_{pg}. Measurement of δ'_{pg} and of the particulate

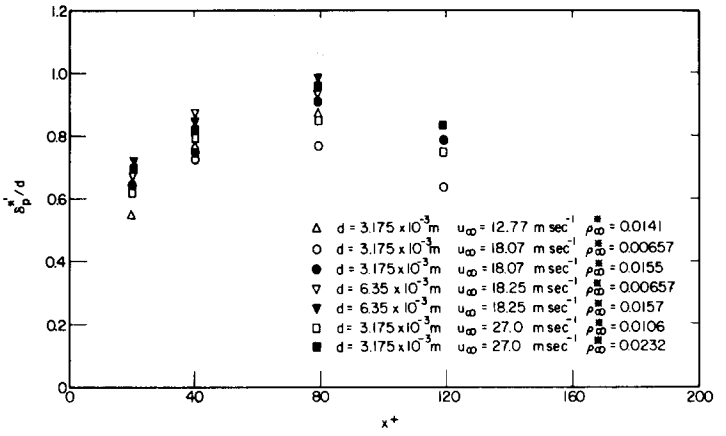

Figure 14. Variation of $\delta_p^{*\prime}$.

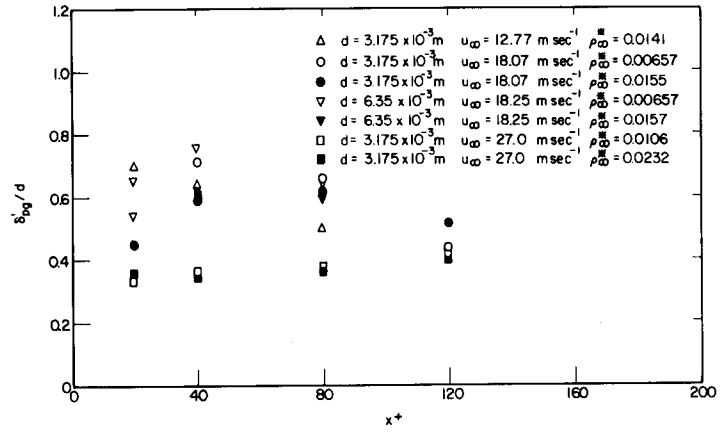

Figure 15. Variation of δ'_{pg}.

density wake half width comply with the constraint predicted by [18] with the possible exception of data for $u_\infty = 27.0\ \mathrm{m\ s^{-1}}$.

The ratio of particulate mass to gaseous mass displaced by the wake was calculated and the results are shown in figure 16. From the data, maximum displacement of particulate material relative to the gas flow occurs at $x/d \simeq 80$. Consequently, this location is suggested if particulate separation and eventual extraction is contemplated through means of wake flow.

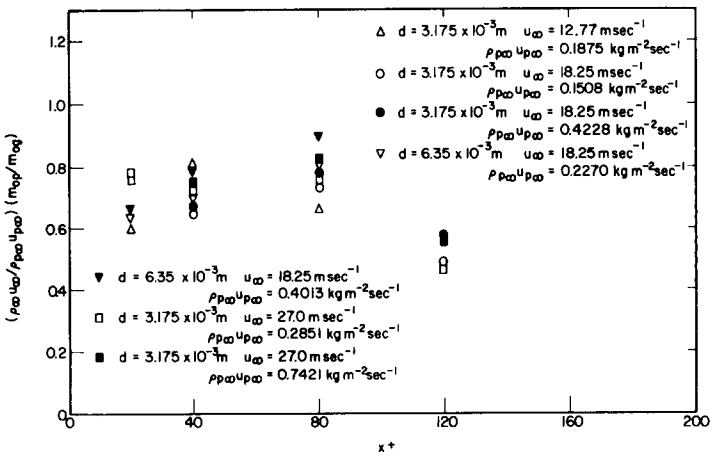

Figure 16. Ratio of particulate mass to gaseous mass displaced by wake.

CONCLUSIONS

All the conclusions are based on the measurements and calculations performed in this work.

1. Geometric origins of similarity for both the particulate momentum and particulate density wakes coincide with the geometric origin of the gaseous wake.

2. Establishment of fully developed conditions along the wake center-line require approximately twice the downstream distance for particulate velocity relative to gaseous velocity. For particulate density along the wake centerline, fully developed conditions are established at less than twice the distance but greater than the distance required for the gaseous velocity.

3. Distribution of particulate momentum and particulate density in the wake region where gaseous similarity is established conforms to Gauss's function. Variation of all transport properties within the central portion of the wake did not exist.

4. Variation of particulate loading has no discernible effect upon gaseous or particulate variables within the wake region.

5. Both the particulate momentum and particulate density wakes are smaller in width than the gaseous wake. The particulate momentum wake width is the least and the particulate density wake width is between the gaseous wake width and particulate momentum wake width. Also, growth of the particulate wake half widths relative to the gaseous wake occurs over the range of measurements.

REFERENCES

DEICH, M. E., FILIPPOR, G. A., SALTANOV, G. A., LAUKHIN, Y. A. & SIVOBOROD, V. A. 1973 Investigation of phase changes in swirling flows of supersaturated vapor. *Fluid Mech., Sov. Res.* **2**, 80–88.

FENTON, D. L. 1974 Flow of a particulate suspension in the wake of a cylinder. Ph.D. Thesis, Department of Mechanical Engineering, University of Illinois at Urbana-Champaign, Urbana IL, pp. 7–17.

FENTON, D. L. & STUKEL, J. J. 1976 Measurement of the local particle concentration in fully turbulent duct flow. *Int. J. Multiphase Flow* **3**, 141–145.

HINZE, J. O. 1959 *Turbulence*, Ch. 6. McGraw-Hill, New York.

MORR, G. F. 1972 The turbulent flow of a suspension over an ellipsoid of revolution. Ph.D. Thesis, Department of Mechanical Engineering, University of Illinois at Urbana-Champaign, Urbana IL, pp. 12–14.

SCHLICHTING, H. 1968 *Boundary-Layer Theory*, 6th Ed., Ch. 15. McGraw-Hill, New York.

TOWNSEND, A. A. 1956 *The Structure of Turbulent Shear Flow*, pp. 131–171. Cambridge University Press, London.